Neurobiology of Aging 59 (2017) 135–143

Contents lists available at ScienceDirect

Neurobiology of Aging

journal homepage: www.elsevier.com/locate/neuaging

Associations between dynamic functional connectivity and age, metabolic risk, and cognitive performance

Raymond P. Viviano [a,b], Naftali Raz [a,b], Peng Yuan [c], Jessica S. Damoiseaux [a,b,*]

[a] Department of Psychology, Wayne State University, Detroit, MI, USA
[b] Institute of Gerontology, Wayne State University, Detroit, MI, USA
[c] School of Kinesiology, University of Michigan, Ann Arbor, MI, USA

ARTICLE INFO

Article history:
Received 7 March 2017
Received in revised form 3 July 2017
Accepted 2 August 2017
Available online 10 August 2017

Keywords:
Resting-state fMRI
Cognitive aging
Executive function
Functional connectivity
Default network

ABSTRACT

Advanced age is associated with reduced within-network functional connectivity, particularly within the default mode network. Most studies to date have examined age differences in functional connectivity via static indices that are computed over the entire blood-oxygen-level dependent time series. Little is known about the effects of age on short-term temporal dynamics of functional connectivity. Here, we examined age differences in dynamic connectivity as well as associations between connectivity, metabolic risk, and cognitive performance in healthy adults (N = 168; age, 18–83 years). A sliding-window k-means clustering approach was used to assess dynamic connectivity from resting-state functional magnetic resonance imaging data. Three out of 8 dynamic connectivity profiles were associated with age. Furthermore, metabolic risk was associated with the relative amount of time allocated to 2 of these profiles. Finally, the relative amount of time allocated to a dynamic connectivity profile marked by heightened connectivity between default mode and medial temporal regions was positively associated with executive functions. Thus, dynamic connectivity analyses can enrich understanding of age-related differences beyond what is revealed by static analyses.

1. Introduction

Aging affects many aspects of brain structure and function and is associated with cognitive decline (see Fjell et al., 2014; Kennedy and Raz, 2015 for recent reviews). Understanding age differences in brain functional organization is an important step in elucidating neural mechanisms of cognitive aging, and since its introduction, resting-state functional magnetic resonance imaging (rs-fMRI; Biswal et al., 1995; Raichle et al., 2001), has been applied to assess age-related differences in brain network functioning. In rs-fMRI analyses, configuration and strength of functional organization is commonly inferred from spatial patterns of temporal correlations between low-frequency fluctuations in blood-oxygen-level dependent (BOLD) signals of different brain regions, termed "functional connectivity" (Biswal et al., 1995; Cordes et al., 2001; Lowe et al., 1998). Many resting-state networks (RSNs) have been identified (Beckmann et al., 2005; Damoiseaux et al., 2006; De Luca et al., 2006; Fox et al., 2005), and the spatial configurations of these RSNs have been comparable to spatial configurations of networks observed during task performance (Calhoun et al., 2008; Smith et al., 2009).

Of the multiple known RSNs, the default mode network (DMN), which is more active during wakeful, task-free rest and less active during overt task engagement, has received extensive attention (Buckner et al., 2008; Greicius et al., 2003; Raichle et al., 2001; Shulman et al., 1997). DMN activity is associated with episodic memory and future planning (Buckner et al., 2008), and DMN connectivity at rest predicts subsequent memory performance (Sala-Llonch et al., 2012; Wang et al., 2010). Furthermore, resting DMN connectivity is negatively related to age (Andrews-Hanna et al., 2007; Damoiseaux et al., 2008; Wu et al., 2011), and, in comparison to younger participants, older adults exhibit lower task-related deactivation of DMN regions (Grady et al., 2006; Lustig et al., 2003; Sambataro et al., 2010). Thus, advanced age may be linked to reduced flexibility in response to task demands. Whole-brain functional connectivity analysis has also revealed age-associated breakdown of communication within RSNs and elevated communication between RSNs (Chan et al., 2014), suggesting age-related dedifferentiation of brain organization.

An important common feature, and possible limitation, of most rs-fMRI studies in healthy adults is reliance on functional connectivity indices calculated from an entire scan session. Potentially important information about within-scan temporal changes in

* Corresponding author at: 87 East Ferry St., Detroit, MI, USA. Tel.: (313) 664-2642; fax: (313) 664-2666.
E-mail address: damoiseaux@wayne.edu (J.S. Damoiseaux).

0197-4580/$ – see front matter © 2017 Elsevier Inc. All rights reserved.
http://dx.doi.org/10.1016/j.neurobiolaging.2017.08.003

functional connectivity may be lost in this aggregation (Allen et al., 2014; Chang and Glover, 2010; Sakoglu et al., 2010). The assessment of dynamic functional connectivity in rs-fMRI (see Hutchinson et al., 2013a, for methodological review) has revealed that individuals may transition between different dynamic whole-brain connectivity profiles (often called "states") characterized by distinct connectivity patterns (Allen et al., 2014). The dynamic connectivity profiles reveal variability in functional brain organization over time. This variability may reflect changes in neural activity related to cognitive and sensorimotor operations, as well as nonneuronal factors such as systemic physiological changes or spontaneous head motion. Previous work suggests that variability in hub region multinetwork participation is lower (Schaefer et al., 2014), and variability within DMN dynamic functional connectivity is higher (Madhyastha and Grabowski, 2014) in older compared to younger adults. Furthermore, stability of functional connectivity increases with age in some regions (e.g., middle frontal gyrus), while decreasing in others (e.g., supramarginal gyrus) (Yin et al., 2016). These patterns of age differences suggest that dynamic properties of brain networks may reflect neural phenomena relevant to age-related functional declines.

Despite growing interest in connectivity dynamics, investigations of lifespan age differences therein remain scarce. Therefore, the present study aimed to determine age-related differences in dynamic functional connectivity and their relation to cognitive performance in healthy adults. We hypothesized age differences in patterns of DMN dynamic connectivity as static connectivity differences within this network have been previously observed (Andrews-Hanna et al., 2007; Damoiseaux et al., 2008; Wu et al., 2011), and increased DMN variability has been noted in older adults (Madhyastha and Grabowski, 2014). Specifically, we hypothesized that time allocation among specific dynamic connectivity profiles would be age dependent and that older adults would devote less time to profiles dominated by strong connectivity within DMN, and between DMN and other networks, compared to younger counterparts. We also hypothesized that time share of specific profiles would be related to cognitive performance, with more "youthful" patterns of dynamic connectivity linked to higher cognitive scores, analogous to associations observed in extant studies of static DMN connectivity and cognition (Sala-Llonch et al., 2012; Wang et al., 2010). Considering reported age-related decreases in dynamic hub-region network variability (Garrett et al., 2010; Schaefer et al., 2014) and increased variability in DMN component intercorrelation (Madhyastha and Grabowski, 2014), we also expected our dynamic analysis to capture age differences in the rate of switching between connectivity profiles. Specifically, we hypothesized older adults would switch profiles at a lower rate, which might reflect less-than-optimal cognitive processing.

2. Methods

2.1. Participants

Structural and functional MRI data were available for 168 adults (61 men, 107 women; 18–83 years, M = 48.8, standard deviation [SD] = 18.0), recruited from the Metro Detroit, Michigan area through advertisements in newspapers and flyers. Participants were enrolled in an ongoing longitudinal study, in which the resting-state sequence was introduced after some had undergone more than 1 wave of testing. Therefore, complete baseline cognitive testing data corresponding to the time of baseline rs-fMRI acquisition were available only for a subsample of 91 participants (33 men, 58 women) with age range 18–78 years (M = 42.2, SD = 17.6). The Wayne State University Institutional Review Board approved the study, and signed informed consent was obtained from all participants. Debriefing followed the experiment. Participants spoke English as their first language and were deemed right-hand dominant after scoring over 75% on the Edinburgh Inventory (Oldfield, 1971). They were screened for neurological, psychiatric, cardiovascular, and endocrine diseases, diabetes, cancer, and a history of loss of consciousness greater than 5 minutes. Participants were also screened for dementia [Mini–Mental State Examination $\geq$26 (Folstein et al., 1975)]; and depression [Center for Epidemiological Study Depression questionnaire $\leq$16; (Radloff, 1977)]. A metabolic risk score was computed as the sum of standardized indicators of metabolic syndrome (Grundy et al., 2004): waist-hip ratio, blood triglycerides, systolic blood pressure, fasting blood glucose, and high-density lipoprotein (reverse coded). See previous report for details (Damoiseaux et al., 2016). Metabolic health indicators were available for 151 of the 168 participants, and 84 of the 91 participants with cognitive data.

2.2. Assessment of cognitive performance

Cognitive tests, described in previous publications (e.g., Raz et al., 2009), were administered across 4 sessions within a 3-month window around the MRI session. We performed confirmatory factor analysis (CFA) to determine the main cognitive constructs. The CFA model consisted of 3 latent factors: processing speed, with letter comparison and pattern comparison scores as indicators; memory, with Woodcock-Johnson-R Memory for Names (WJR memory, immediate and delayed) scores as indicators; and executive functioning, with the following indicators: Stroop, Wisconsin Card Sorting Test, size judgment span, listening span, spatial recall, and Cattell Culture Fair Test (form 3B, tests 1, 2, 3, 4). Analyses were conducted with Mplus 6.0 (Muthén and Muthén), and composite factor scores were calculated for each latent factor (see Damoiseaux et al., 2016 for a detailed description of the CFA).

2.3. MRI data acquisition

Imaging was performed at the Wayne State University MRI research facility on a 3-Tesla Siemens Verio (Siemens Medical AG, Erlangen, Germany) full-body magnet with a 12-channel head coil. For the resting-state functional scan, 200 volumes of 43 axial slices were acquired using a T2*-weighted echo planar sequence: repetition time (TR) = 2500 ms, echo time = 30 ms, flip angle = 90°, pixel bandwidth = 2298 Hz/pixel, generalized autocalibrating partial parallel acquisition acceleration factor phase-encoding = 2, field-of-view = 210 mm, matrix size = 64 × 64, and voxel size = 3.3 × 3.3 × 3.3 mm. Participants were instructed to remain still with eyes open. For the anatomical scan, a 3D T1-weighted magnetization-prepared rapid gradient-echo sequence was acquired: TR = 1680 ms; echo time = 3.51 ms; inversion time = 900 ms; flip angle = 9.0°, pixel bandwidth = 180 Hz/pixel, generalized autocalibrating partial parallel acquisition = 2; field-of-view = 256 mm, matrix size = 384 × 384, and voxel size 0.67 × 0.67 × 1.34 mm.

2.4. Preprocessing

Image preprocessing was carried out with the FMRIB Software Library (version 5.0; Smith et al., 2004). Resting-state processing included removal of the first 4 image volumes, motion correction (Jenkinson et al., 2002), removal of nonbrain structures (Smith, 2002), spatial smoothing (6 mm FWHM), 4D grand-mean scaling, and high-pass temporal filtering (Gaussian-weighted least-squares straight line fitting, sigma = 150.0 seconds). The scan was then aligned with the corresponding high-resolution T1 and subsequently registered to 3-mm isotropic MNI152 space

with affine linear registration (Jenkinson et al., 2002). Translation and rotation time courses were regressed from the images to attenuate the influence of head motion on results. Participants with more than 3 mm absolute head displacement during the scan were not included in the analysis. Global signal contribution was removed.

2.5. ROI generation and organization

One hundred seventy-five regions of interest (ROIs) were defined from a group-level parcellation generated with spatially constrained normalized-cut spectral clustering (Craddock et al., 2012) restricted to a gray matter mask segmented from a Montreal Neurological Institute image using FMRIB Software Library's FAST (Zhang et al., 2001). Of the available ROIs, 172 were used for subsequent analysis after the removal of brain stem ROIs. Mean ROI time series were calculated and assigned a unit variance before covariance estimations. Therefore, subsequent covariance calculations were tantamount to correlation.

Static whole-brain covariance matrices were computed for all participants, Fisher z-transformed, and averaged. A weighted, undirected graph was constructed with ROIs as nodes and the top 10% of positive connections, in terms of strength, as edges. ROIs were organized into nonoverlapping communities with Infomap to define network structure (Lancichinetti and Fortunato, 2009; Rosvall and Bergstrom, 2008). To ensure that the network structure was derived from reliable, strong connectivity, only the top 10% of positive connections were included in the Infomap community detection. Global signal regression, which was applied as a preprocessing step, may induce anticorrelation between networks (Murphy et al., 2009), rendering the interpretation of negative correlations difficult. The Infomap analysis converged on 8 communities (further referred to as RSNs), which after visual inspection were labeled as DMN, sensorimotor (SM), visual (Vis.), dorsal/lateral temporal (dLTL), ventral/medial temporal (vMTL), cerebellar (CB), subcortical (SC), and orbitofrontal (OF; Fig. 1). DMN included medial prefrontal, posterior and anterior cingulate, precuneus, inferior parietal, dorsolateral prefrontal, and rostro-lateral prefrontal cortex. SM included premotor, primary motor, and primary somatosensory cortex. dLTL included Wernicke's area, Broca's area, superior and middle temporal, auditory, parietal, and secondary somatosensory cortex. vMTL included inferior temporal, fusiform, and parahippocampal cortex, hippocampus, and amygdala. SC included thalamus, basal ganglia, and mammillary bodies. CB corresponded to the cerebellum, OF to the orbitofrontal cortex, and Vis. to the occipital cortex.

2.6. Static connectivity analysis

Average static within- and between-network connectivity, calculated as average covariance between ROIs in the same RSN or between ROIs in different RSNs, was computed for each participant. In addition, connectivity within the DMN and between the DMN and other networks was assessed. Multiple linear regression was used to evaluate possible relationships between static network connectivity and age, gender, and metabolic risk. Based on previous findings (La Joie et al., 2014; Wang et al., 2010), we also evaluated the associations of within-DMN connectivity and DMN-vMTL connectivity with cognitive performance, while controlling for age, gender, and metabolic risk.

2.7. Dynamic covariance calculation

Dynamic connectivity was assessed via sliding-window k-means clustering, after Allen et al. (2014). Covariance matrices were estimated from regularized precision matrices (Smith et al., 2011; Varoquaux et al., 2010) computed from windowed segments of the mean ROI time series (Tukey window; width = 28 TR or 70 seconds, alpha = 0.2, step size = 7 TR). Window width and step size were chosen based on published research (Hutchison et al., 2013b; Shirer et al., 2012), with the aim of reducing autocorrelation between successive windows and retaining adequate power to detect dynamic connectivity patterns. Regularization was carried out via group sparse covariance estimation (Varoquaux et al., 2010) with NiLearn (based on the scikit-learn package; Abraham et al., 2014; Pedregosa et al., 2011). Regularization was optimized for each participant independently; the estimator was fit on a participant's set of covariance matrices by assessing the likelihood of unseen matrices through leave-one-out cross-validation. Matrices were Fisher z-transformed after estimation.

We applied k-means clustering (Lloyd, 1982), using L1 distance (Aggarwal et al., 2001), to the set of all dynamic covariance matrices to identify consistent and differing dynamic connectivity patterns. K-means analysis was repeated with the number of clusters (k) ranging from 2 to 9 and run 500 times at each level of k to escape local minima. The final number of clusters, $k = 8$, was determined by the gap statistic (Tibshirani et al., 2001) with 50 generated reference samples. After determining k, the data were bootstrap-resampled 50 times and clustered the same way as the original data to assess stability of clusters via Jaccard similarity (Hennig, 2007). For each cluster in the original set, the similarity value between that cluster and the most similar cluster in the bootstrapped set was recorded. Maximum similarities over all 50 resampling rounds were averaged for each cluster (Table S1).

2.8. Dynamic connectivity profile quantification

Modularity was calculated twice for each dynamic connectivity profile (Rubinov and Sporns, 2011): once using the static network definition and once with a network structure determined by applying Infomap to the dynamic centroid. Modularity of a profile given the static network definition was interpreted as representing proximity of the modular structure of the dynamic profile to static structure. Modularity given dynamic network structure was interpreted as indication that a modular structure was present even if dynamic and static structures did not correspond.

Average whole-brain within- and between-network connectivity, as well as average connectivity within the DMN and between the DMN and the rest of the brain, were compared between each dynamic connectivity profile and the static profile with independent samples t tests (Table 1). Independent samples t tests were also used to compare each connection in the dynamic connectivity profiles to the corresponding connection in the static profile to assess individual ROI pairing connectivity differences (Fig. S1). Dynamic connectivity profiles were also assessed qualitatively by plotting radial tree graphs of the top 10% of positive connections of the centroids (Fig. 2).

2.9. Associating dynamic connectivity with age, gender, and metabolic risk

Having a portion of a scan allocated to a dynamic connectivity profile was treated for each participant as a binary outcome—1 for having and 0 for not having. We used logistic regression to investigate the impact of age, gender, and metabolic risk on that outcome for each profile. The number of unique connectivity profiles and transitions between profiles per participant was also noted. Linear regression assessed the associations between age and metabolic risk with the number of

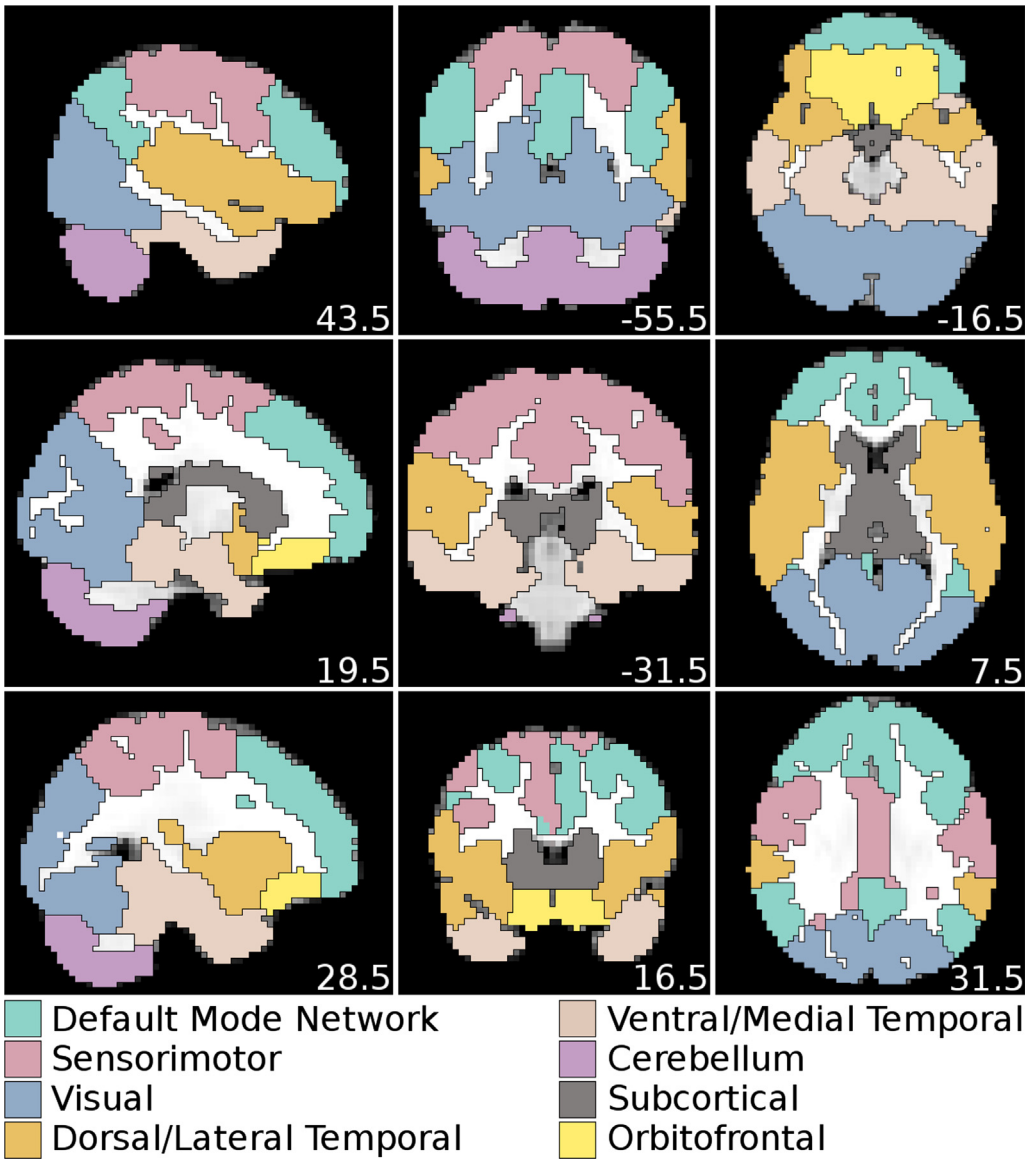

Fig. 1. ROI network structure after running Infomap on the static FC graph of the 90th percentile of positive connections. Eight ROI subgraphs were detected by Infomap. Coordinates are in MNI space. MNI, Montreal Neurological Institute.

unique dynamic profiles and the relationship between age and number of transitions.

Vectors indicating to which dynamic connectivity profile each windowed covariance matrix belonged were created for each participant. The amount of time allocated to each dynamic connectivity profile was then calculated and multiple linear regression was performed to examine the influences of age, gender, and metabolic risk on the relative amount of time allocated to a profile. Participants who did not have a portion of their scan correspond to a profile were not included in that regression; therefore, each analysis drew a different subsample of the participant pool.

2.10. Associating dynamic connectivity with cognitive performance

The event of allocating any time to a particular profile was related to cognitive performance in the subset of 91 participants while controlling for age, gender, and metabolic risk via analysis of covariance. For participants who had some portion of their scan correspond to a profile, the relative amount of time allocated to that profile was related to cognitive performance constructs via general linear models with age, gender, and metabolic risk included. Only connectivity profiles 2, 3, and 7 were evaluated because too few participants with metabolic and cognitive data had connectivity patterns related to the other profiles ($n << 40$).

2.11. Packages, visualizations, and multiple comparison correction

In-house Python (2.7.6) and R (3.3.1) scripts, and SPSS (23.0), were used for statistical analyses, FSLView was used for ROI RSN structure visualization, graph-tool (Peixoto, 2014) was used for radial tree graph visualization, and matplotlib (Hunter, 2007) was used for all other visualizations. Experiment-wise false discovery rate correction ($q = 5\%$) was applied. Matrices comparing each static connection to the corresponding dynamic connections were not included in this false discovery rate correction and were instead Bonferroni corrected ($\alpha = 3.39E\text{-}6$) on a per-matrix basis.

Table 1
Within- and between-network average connectivity differences between the static connectivity profile and dynamic connectivity profiles

	Overall within	Overall between	DMN within	DMN between
Static	0.2601	−0.0265	0.2074	−0.0293
Profile 1	0.4205	−0.0332	0.3199	−0.0575
$t(410)$	−15.12	4.9274	−8.3144	7.7877
p	[b]<0.0001	[b]<0.0001	[b]<0.0001	[b]<0.0001
Profile 2	0.2371	−0.0234	0.1786	−0.0261
$t(1485)$	4.5141	−5.1539	4.7751	−1.9272
p	[b]<0.0001	[b]<0.0001	[b]<0.0001	0.0549
Profile 3	0.3048	−0.0278	0.2417	−0.0395
$t(775)$	−6.8210	1.6469	−4.2732	4.2302
p	[b]<0.0001	0.1008	[b]<0.0001	[b]<0.0001
Profile 6	0.3582	−0.0298	0.3123	−0.0262
$t(417)$	−10.4580	3.0395	−9.4912	−1.0227
p	[b]<0.0001	[b]0.0026	[b]<0.0001	0.3076
Profile 7	0.2668	−0.0252	0.2492	−0.0224
$t(984)$	−1.1698	−2.0326	−6.0450	−3.7135
p	0.2431	[a]0.0430	[b]<0.0001	[b]0.0002
Profile 8	0.3011	−0.0277	0.2624	−0.0220
$t(627)$	−5.7559	1.3968	−5.9295	−3.1728
p	[b]<0.0001	0.1638	[b]<0.0001	[b]0.0017

Two-tailed independent samples t tests. Negative t values indicate that the average connectivity was greater in the dynamic profile.
Key: DMN, default mode network.
[a] Significant at $\alpha = 0.05$.
[b] Significant after experiment-wise false discovery rate correction.

3. Results

3.1. Static functional connectivity

Advanced age was associated with lower functional connectivity between DMN and vMTL ($\beta = -0.282$, $p = 0.001$), and greater connectivity between DMN and SM ($\beta = 0.222$, $p = 0.01$), while controlling for metabolic risk and gender. Women, regardless of age or network type, had lower average within ($\beta = -0.239$, $p = 0.008$) and between ($\beta = -0.233$, $p = 0.01$) network connectivity compared to men.

3.2. Dynamic functional connectivity and its correlates

3.2.1. Connectivity profiles

Eight dynamic connectivity profiles identified in these data are depicted in Fig. 2. Not every participant entered each profile, and the mean number of profiles per person was 3.12 (SD = 1.00). Dynamic connectivity profiles 2, 3, and 7 had high membership, whereas the rest had moderate to low membership, particularly profile 4 (Table S1). All connectivity profiles, except profile 5, exhibited moderate (greater than 0.5) to high (greater than 0.7) average Jaccard values, indicating cluster stability (Table S1). Less stable profiles could reflect important between-subject variability, but also intermediate transitional states between more stable profiles. No profile represented a dissolved network configuration as all had moderate modularity given a network structure optimized for the profile centroid (Table S1). Because of low membership and low stability, profiles 4 and 5 were removed from further analyses. Differences between the remaining dynamic connectivity profiles and the static profile in whole brain and DMN-specific within- and between-network connectivity are detailed in Table 1 and depicted in Fig. S1.

3.2.2. Predictors of connectivity profile presence

Differences in the presence or absence of a connectivity profile may indicate differences in brain network organization and efficiency. We therefore applied logistic regression to test age, gender, and metabolic risk as predictors of individual dynamic connectivity profile membership (Table S2). Older age was associated with lower odds of having profiles 2 (odds ratio [OR] = 0.957, $p = 0.005$) and 7 (OR = 0.953, $p < 0.0001$) and higher odds of having profile 3 (OR = 1.028, $p = 0.008$). Neither metabolic risk nor gender was associated with any of the dynamic profiles. The age difference in odds of having profiles 3 and 7 is in accord with our finding of lower DMN-vMTL connectivity in older adults in the static functional connectivity analysis, because profile 3 has low whereas profile 7 has high DMN-vMTL between-network connectivity (Fig. 2). Since the connectivity pattern of profile 2 is most similar to the static connectivity pattern (Fig. S1), lower odds of the observing profile 2 could be interpreted as an age-related deviation from typical brain integration.

3.2.3. Number of unique connectivity profiles and profile transitions

The number of unique dynamic connectivity profiles per individual was unrelated to age or metabolic risk ($R^2 = 0.004$, $p = 0.72$; age $\beta = -0.07$, $p = 0.43$; metabolic risk $\beta = 0.006$, $p = 0.94$). Moreover, we observed no association between the number of profile transitions and age ($R^2 = 0.005$, age $\beta = -0.07$, $p = 0.35$). This was contrary to our expectations that older adults would have lower transition rates.

3.2.4. Age, gender, metabolic risk, and relative time allocated to dynamic connectivity profiles

Older age was associated with more time allocated to profile 8 ($\beta = 0.357$, $p = 0.009$), that evidenced lesser connectivity between DMN and SM, Vis., and dLTL, and greater DMN-CB and DMN-SC connectivity compared to the static profile (Fig. S1). Furthermore, greater metabolic risk score was associated with more time allocated to profile 2 ($\beta = 0.278$, $p = 0.007$) and less time to profile 7 ($\beta = -0.350$, $p = 0.003$). None of the other tested associations reached significance (see Table S3).

3.2.5. Cognitive performance and functional connectivity

Whether an individual exhibited a specific dynamic profile or not was unrelated to cognitive performance after controlling for age, gender, and metabolic risk. However, the relative amount of time allocated to profile 7 was positively associated with executive function score ($\beta = 0.297$, $p = 0.013$) for participants who had that pattern of connectivity. Thus, the more time participants allocated to a dynamic connectivity pattern with high DMN connectivity, the better their performance was on tasks of executive functioning outside of the scanner. None of the other tested associations between time allocated to a profile and cognitive function reached significance (Table S4). Furthermore, static DMN connectivity was unrelated to cognitive performance beyond age, gender, and metabolic risk (Tables S5 and S6).

3.2.6. Effect of motion on dynamic functional connectivity

Motion artifacts can remain in the signal time series after motion regression (Power et al., 2012), and dynamic connectivity could be influenced by head motion (Laumann et al., 2016). Assessment of the association between head motion and dynamic functional connectivity in our data revealed that mean framewise displacement (FD) was associated with odds of demonstrating any profile except profile 8 and with time allocated to profile 2 (Tables S7 and S8). Mean FD was unrelated to rate of switching between profiles ($r = 0.14$, $p = 0.06$). The observed age, gender, and metabolic risk effects remained largely the same after including

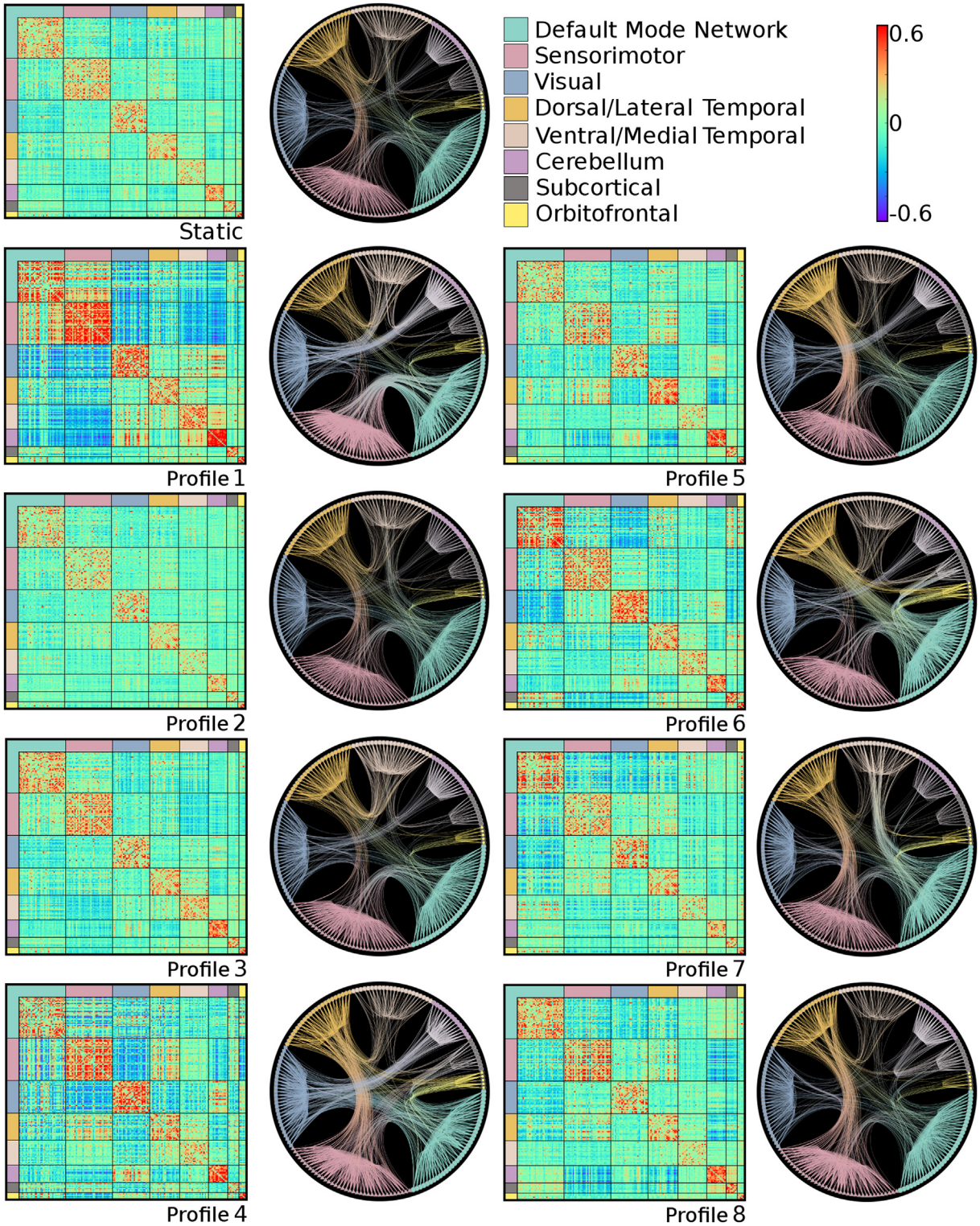

Fig. 2. Functional connectivity for the static connectivity profile and each dynamic connectivity profile. Matrices represent average positive and negative connectivity between ROIs for all participants (static only) or average positive and negative connectivity between ROIs for all windows that correspond to a dynamic profile. Radial tree graphs represent the 90th percentile of positive connections.

mean FD into the models. Only the age-related odds of demonstrating profile 2 were reduced to a trend level, and age-related odds of demonstrating profile 3 were no longer significant (Table S7).

4. Discussion

We examined age-related differences in dynamic functional connectivity and contrasted the results to findings obtained from a

static connectivity analysis. In line with previous research, we found lower static functional connectivity between default mode regions and ventral and medial regions of the temporal lobe in older participants (Andrews-Hanna et al., 2007; Damoiseaux et al., 2016). This lower static DMN-vMTL connectivity may represent an age-related reduction in communication within putative memory systems (Ranganath and Ritchey, 2012). Projections from MTL regions to posterior DMN regions are part of a presumed posterior memory system, which is thought to be involved in episodic memory function (Kahn et al., 2008; Ranganath and Ritchey, 2012). Our finding of gender differences in static whole-brain within- and between-network connectivity is in accord with previous reports of gender differences across functional connectivity measures (Gong et al., 2011; Tomasi and Volkow, 2012). Because of the association between gender and functional connectivity, we included gender in the models, but the results remained significant after this control. No gender differences were observed in the dynamic connectivity measures.

4.1. Dynamic resting functional connectivity

After partitioning the total BOLD time series into discrete segments, we found that older participants were less likely to allocate windowed time segments to a dynamic connectivity profile similar to the static state (profile 2) and a profile with high DMN-vMTL connectivity (profile 7) but more likely to allocate them to a profile with low DMN-vMTL connectivity (profile 3). These findings suggest that the lower connectivity observed in the static state can be explained by both lower and higher odds of having certain transient connectivity profiles.

Connectivity profile 2 has the highest membership of all profiles (i.e., present in 132 participants and accounted for 31.4% of all windows; Table S1) and is most similar to the static state (Fig. S1). Therefore, this connectivity pattern may reflect a kind of "ground state" with other profiles possibly reflecting deviations from it that arise due to cognition, movement in the scanner (Laumann et al., 2016; Power et al., 2012; Van Dijk et al., 2012), sleep (Allen et al., 2014), or respiration and variations in arterial blood flow (Chang and Glover, 2010; Wise et al., 2004). The lower odds of having certain profiles in older adults could reflect known age-related differences observed using static connectivity approaches (Andrews-Hanna et al., 2007; Campbell et al., 2013; Damoiseaux et al., 2008, 2016), with the age differences observed in profiles 3 and 7 providing additional information. The lower DMN-vMTL connectivity of profile 3 could indicate disconnection of posterior memory regions, which appears more prevalent in older adults. Conversely, connectivity in profile 7 possibly represents a strengthening or integration of anterior and posterior memory regions as it exhibits greater connectivity between not just DMN and vMTL but also between DMN and OF and vMTL and OF regions (Fig. S1). Projections from MTL to OF regions are considered part of an anterior memory system (Ranganath and Ritchey, 2012).

Profile 7 is of interest in the context of cognitive aging. The association of the profile with lesser metabolic risk and better performance on executive functions suggests that modulation of the DMN by vMTL activity may be important in mitigating decline in typical age-sensitive cognitive domains (Yuan and Raz, 2014) and resisting negative influence of metabolic risk on cognition (Dahle et al., 2009). Both are aspects of aging that are increasingly viewed as mutually related determinants of late-life development (Allan et al., 2016). This is in accord with the extant reports that age-related DMN alterations at rest may be related to age-sensitive cognitive skills (Andrews-Hanna et al., 2007; Damoiseaux et al., 2008). Low membership of profile 7, therefore, may represent a marker for cognitive impairment. An unknown mechanism related to aging or metabolic risk might be preventing maintenance of this connectivity pattern at rest. Conversely, time allocation to profile 7 could be an indicator of cognitive reserve (Stern, 2002). Either way, longitudinal analysis is necessary to determine the relationship between change in cognitive performance and maintenance of dynamic connectivity patterns like profile 7.

Our results indicate that although individuals, regardless of age, can traverse multiple dynamic connectivity profiles, the odds of allocating time to a specific connectivity pattern vary with age. However, contrary to our expectations, we did not observe any association between older age and rate of switching between dynamic connectivity profiles. Because dynamic hub-region network variability decreases with age (Garrett et al., 2010; Schaefer et al., 2014), we hypothesized that functional connectivity patterns would be more similar across shorter periods for older adults. Contrary to this expectation, we found no association between age and the rate of profile switching. Possible explanations for this discrepancy may include differences in analysis approach and sample characteristics, such as exact age range and participant health, between the studies. It is also important to note that, regardless of the observed age-related differences, most of the associations tested did not reveal significant differences. Therefore, the stability of age differences in dynamic functional connectivity remains unclear, and their magnitude may be relatively modest.

4.2. Limitations

Some of the identified connectivity profiles (e.g., profile 4) had low membership, a fact that may confound interpretation. It is possible that clusters with low membership are generalizable and that scanning conditions could be keeping most participants from entering those profiles. Those profiles, however, may also reflect artifacts that confound individual variability in connectivity.

One of the limitations of k-means clustering is the "curse of dimensionality." As clustering algorithms are forced to classify a vast number of connections associated with whole-brain connectivity, dimensionality of a space grows, and empty space between data points increases exponentially. Such disproportionate increase in sparsity can jeopardize the effectiveness of k-means analysis, thus casting doubt on whether obtained clusters optimally represent a true configuration. Most clusters in the present analysis were stable and can therefore be interpreted as meaningful even if not representative of the "true" dynamic connectivity. Still, future analyses could assess dynamic interactions between select regions rather than attempting to quantify the whole brain to overcome dimensionality woes.

Furthermore, the use of group least absolute shrinkage and selection operator (LASSO) regression (Varoquaux et al., 2010) to enforce covariance sparsity on participants individually comes with caveats. Group LASSO forces the same sparsity structure on the set of input covariance matrices. Each participant therefore is assigned their own sparsity structure. Because we expect dynamic connectivity profiles to reveal different connectivity patterns, the "true" underlying sparsity structure between windows may differ. Therefore, applying LASSO is associated with a trade-off: attenuation of covariance estimation error comes with reduction of differences between connectivity profiles—that is, LASSO might artificially make dynamic profiles more similar.

Simulation studies have raised concerns regarding the utility of sliding window approaches to assessing dynamic functional connectivity (Hindriks et al., 2016; Shakil et al., 2016). Future analysis is needed to establish optimal parameters and use of this approach. Dynamic patterns could also be contaminated by head motion (Laumann et al., 2016), and motion artifacts remain in the signal time course even after adjustment via motion regression

(Power et al., 2012); therefore, it is possible that static age-related connectivity differences and the age-related odds of having a specific dynamic connectivity profile could be related to the same motion artifacts. To address this possibility, we assessed the association between mean FD and odds of demonstrating a profile, time allocated to a profile, and rate of switching between profiles. We found that motion was associated with the odds of demonstrating, and the time allocated to, certain profiles. However, observed age, gender, and metabolic risk effects remained largely the same. Thus, although motion is associated with dynamic functional connectivity (FC), it does not fully explain the relationship between dynamic FC, age, and metabolic risk.

It is also suggested that dynamic connectivity reflects systematic and reoccurring patterns of cerebral blood flow that might represent optimized global metabolic processing (Zalesky et al., 2014). However, given that machine learning classifiers can reliably discern between connectivity profiles that arise due to different task demands (Shirer et al., 2012), it is likely that unsupervised algorithms produce meaningful connectivity clusters that provide interesting information about the brain at rest that relates to cognitive functioning.

In this study, we used rs-fMRI data to assess the effect of age on dynamic functional connectivity. It is possible that dynamic functional connectivity assessed during task-evoked functional MRI could yield slightly different results. As observed in the extant literature, static functional connectivity differences exist across different conditions (Shirer et al., 2012) although network connectivity structure remains similar (Smith et al., 2009). Therefore, our prediction regarding the effect of age on DMN connectivity would hold for task-evoked MRI data, even though specific profiles may look different. Nevertheless, more research comparing functional MRI data acquired under different conditions is needed to examine the effect of behavioral context.

5. Conclusion

We observed age-related differences in configuration of dynamic whole-brain functional connectivity patterns at rest. Advanced age, elevated metabolic risk, and low executive function scores were associated with lesser likelihood of a dynamic profile that is characterized by heightened functional connectivity between DMN and vMTL. Lower membership in specific dynamic profiles may denote a potential marker for age-related cognitive decline. Our results indicate that dynamic analysis can capture nuanced differential age-related FC patterns that are obscured by aggregation of BOLD data over the whole time series.

Disclosure statement

The authors have no actual or potential conflicts of interest.

Acknowledgements

This work was supported by grant R37 AG011230 from the National Institutes of Health to NR. The authors thank Cheryl Dahle, Andrew Bender, Ana Daugherty, and Yiqin Yang for assistance in data collection and management.

Appendix A. Supplementary data

Supplementary data associated with this article can be found, in the online version, at http://dx.doi.org/10.1016/j.neurobiolaging.2017.08.003.

References

Abraham, A., Pedregosa, F., Eickenberg, M., Gervais, P., Mueller, A., Kossaifi, J., Gramfort, A., Thirion, B., Varoquaux, G., 2014. Machine learning for neuroimaging with scikit-learn. Front Neuroinform 8, 14.
Aggarwal, C.C., Hinneburg, A., Keim, D.A., 2001. On the surprising behavior of distance metrics in high dimensional space. Lect Notes Comput. Sc 1973, 420–434.
Allan, J.L., McMinn, D., Daly, M., 2016. A Bidirectional relationship between executive function and health behavior: Evidence, Implications, and future Directions. Front Neurosci-switz 10.
Allen, E.A., Damaraju, E., Plis, S.M., Erhardt, E.B., Eichele, T., Calhoun, V.D., 2014. Tracking whole-brain connectivity dynamics in the resting state. Cereb. Cortex 24, 663–676.
Andrews-Hanna, J.R., Snyder, A.Z., Vincent, J.L., Lustig, C., Head, D., Raichle, M.E., Buckner, R.L., 2007. Disruption of large-scale brain systems in advanced aging. Neuron 56, 924–935.
Beckmann, C.F., DeLuca, M., Devlin, J.T., Smith, S.M., 2005. Investigations into resting-state connectivity using independent component analysis. Philos. T Roy Soc. B 360, 1001–1013.
Biswal, B., Yetkin, F.Z., Haughton, V.M., Hyde, J.S., 1995. Functional connectivity in the motor cortex of resting human brain using echo-planar MRI. Magnet Reson. Med. 34, 537–541.
Buckner, R.L., Andrews-Hanna, J.R., Schacter, D.L., 2008. The brain's default network - anatomy, function, and relevance to disease. Ann. Ny Acad. Sci. 1124, 1–38.
Calhoun, V.D., Kiehl, K.A., Pearlson, G.D., 2008. Modulation of temporally coherent brain networks estimated using ICA at rest and during cognitive tasks. Hum. Brain Mapp. 29, 828–838.
Campbell, K.L., Grigg, O., Saverino, C., Churchill, N., Grady, C.L., 2013. Age differences in the intrinsic functional connectivity of default network subsystems. Front Aging Neurosci. 5.
Chan, M.Y., Park, D.C., Savalia, N.K., Petersen, S.E., Wig, G.S., 2014. Decreased segregation of brain systems across the healthy adult lifespan. Proc. Natl. Acad. Sci. U. S. A. 111, E4997–E5006.
Chang, C., Glover, G.H., 2010. Time-frequency dynamics of resting-state brain connectivity measured with fMRI. Neuroimage 50, 81–98.
Cordes, D., Haughton, V.M., Arfanakis, K., Carew, J.D., Turski, P.A., Moritz, C.H., Quigley, M.A., Meyerand, M.E., 2001. Frequencies contributing to functional connectivity in the cerebral cortex in "resting-state" data. Am. J. Neuroradiol 22, 1326–1333.
Craddock, R.C., James, G.A., Holtzheimer, P.E., Hu, X.P.P., Mayberg, H.S., 2012. A whole brain fMRI atlas generated via spatially constrained spectral clustering. Hum. Brain Mapp. 33, 1914–1928.
Dahle, C.L., Jacobs, B.S., Raz, N., 2009. Aging, Vascular risk, and cognition: blood glucose, Pulse pressure, and cognitive performance in healthy adults. Psychol. Aging 24, 154–162.
Damoiseaux, J.S., Beckmann, C.F., Arigita, E.J.S., Barkhof, F., Scheltens, P., Stam, C.J., Smith, S.M., Rombouts, S.A.R.B., 2008. Reduced resting-state brain activity in the "default network" in normal aging. Cereb. Cortex 18, 1856–1864.
Damoiseaux, J.S., Rombouts, S.A.R.B., Barkhof, F., Scheltens, P., Stam, C.J., Smith, S.M., Beckmann, C.F., 2006. Consistent resting-state networks across healthy subjects. Proc. Natl. Acad. Sci. U. S. A. 103, 13848–13853.
Damoiseaux, J.S., Viviano, R.P., Yuan, P., Raz, N., 2016. Differential effect of age on posterior and anterior hippocampal functional connectivity. Neuroimage 133, 468–476.
De Luca, M., Beckmann, C.F., De Stefano, N., Matthews, P.M., Smith, S.M., 2006. fMRI resting state networks define distinct modes of long-distance interactions in the human brain. Neuroimage 29, 1359–1367.
Fjell, A.M., McEvoy, L., Holland, D., Dale, A.M., Walhovd, K.B., Initi, A.s.D.N., 2014. What is normal in normal aging? Effects of aging, amyloid and Alzheimer's disease on the cerebral cortex and the hippocampus. Prog. Neurobiol. 117, 20–40.
Folstein, M.F., Folstein, S.E., Mchugh, P.R., 1975. Mini-mental state - Practical method for grading cognitive state of Patients for Clinician. J. Psychiat Res. 12, 189–198.
Fox, M.D., Snyder, A.Z., Vincent, J.L., Corbetta, M., Van Essen, D.C., Raichle, M.E., 2005. The human brain is intrinsically organized into dynamic, anticorrelated functional networks. Proc. Natl. Acad. Sci. U. S. A. 102, 9673–9678.
Garrett, D.D., Kovacevic, N., McIntosh, A.R., Grady, C.L., 2010. Blood oxygen level-dependent signal variability is more than just Noise. J. Neurosci. 30, 4914–4921.
Grady, C.L., Springer, M.V., Hongwanishkul, D., McIntosh, A.R., Winocur, G., 2006. Age-related changes in brain activity across the adult lifespan. J. Cogn. Neurosci. 18, 227–241.
Gong, G., He, Y., Evans, A.C., 2011. Brain connectivity: gender makes a difference. Neuroscientist 17, 575–591.
Greicius, M.D., Krasnow, B., Reiss, A.L., Menon, V., 2003. Functional connectivity in the resting brain: a network analysis of the default mode hypothesis. Proc. Natl. Acad. Sci. U. S. A. 100, 253–258.
Grundy, S.M., Brewer, H.B., Cleeman, J.I., Smith, S.C., Lenfant, C. Participants, C, 2004. Definition of metabolic syndrome - report of the National Heart, Lung, and blood Institute/American Heart association Conference on Scientific issues related to definition. Circulation 109, 433–438.
Hennig, C., 2007. Cluster-wise assessment of cluster stability. Comput. Stat. Data 52, 258–271.
Hindriks, R., Adhikari, M.H., Murayama, Y., Ganzetti, M., Mantini, D., Logothetis, N.K., Deco, G., 2016. Can sliding-window correlations reveal dynamic functional connectivity in resting-state fMRI? Neuroimage 127, 242–256.

Hunter, J.D., 2007. Matplotlib: a 2D graphics environment. Comput. Sci. Eng. 9, 90–95.
Hutchison, R.M., Womelsdorf, T., Allen, E.A., Bandettini, P.A., Calhoun, V.D., Corbetta, M., Penna, S., Duyn, J.H., Glover, G.H., Gonzalez-Castillo, J., Handwerker, D.A., Keilholz, S., Kiviniemi, V., Leopold, D.A., Pasquale, F., Sporns, O., Walter, M., Chang, C., 2013a. Dynamic functional connectivity: Promise, issues, and interpretations. Neuroimage 80, 360–378.
Hutchison, R.M., Womelsdorf, T., Gati, J.S., Everling, S., Menon, R.S., 2013b. Resting-state networks show dynamic functional connectivity in awake humans and anesthetized macaques. Hum. Brain Mapp. 34, 2154–2177.
Jenkinson, M., Bannister, P., Brady, M., Smith, S., 2002. Improved optimization for the robust and accurate linear registration and motion correction of brain images. Neuroimage 17, 825–841.
Kahn, I., Andrews-Hanna, J.R., Vincent, J.L., Snyder, A.Z., Buckner, R.L., 2008. Distinct cortical anatomy linked to subregions of the medial temporal lobe revealed by intrinsic functional connectivity. J. Neurophysiol. 100, 129–139.
Kennedy, K., Raz, N., 2015. Normal aging of the Brain, Brain Mapping: An Encyclopedic Reference. Academic Press, Elsevier Cambridge, pp. 603–617.
La Joie, R., Landeau, B., Perrotin, A., Bejanin, A., Egret, S., Pelerin, A., Mezenge, F., Belliard, S., de la Sayette, V., Eustache, F., Desgranges, B., Chetelat, G., 2014. Intrinsic connectivity Identifies the Hippocampus as a main Crossroad between Alzheimer's and Semantic dementia-Targeted networks. Neuron 81, 1417–1428.
Lancichinetti, A., Fortunato, S., 2009. Community detection algorithms: a comparative analysis. Phys. Rev. E 80.
Laumann, T.O., Snyder, A.Z., Mitra, A., Gordon, E.M., Gratton, C., Adeyemo, B., Gilmore, A.W., Nelson, S.M., Berg, J.J., Greene, D.J., McCarthy, J.E., Tagliazucchi, E., Laufs, H., Schlaggar, B.L., Dosenbach, N.U., Petersen, S.E., 2016. On the stability of BOLD fMRI correlations. Cereb. Cortex 1–14. http://dx.doi.org/10.1093/cercor/bhw265.
Lloyd, S.P., 1982. Least-squares Quantization in Pcm. Ieee T Inform Theor. 28, 129–137.
Lowe, M.J., Mock, B.J., Sorenson, J.A., 1998. Functional connectivity in single and multislice echoplanar imaging using resting-state fluctuations. Neuroimage 7, 119–132.
Lustig, C., Snyder, A.Z., Bhakta, M., O'Brien, K.C., McAvoy, M., Raichle, M.E., Morris, J.C., Buckner, R.L., 2003. Functional deactivations: change with age and dementia of the Alzheimer type. Proc. Natl. Acad. Sci. U. S. A. 100, 14504–14509.
Madhyastha, T.M., Grabowski, T.J., 2014. Age-related differences in the dynamic architecture of intrinsic networks. Brain Connect 4, 231–241.
Murphy, K., Birn, R.M., Handwerker, D.A., Jones, T.B., Bandettini, P.A., 2009. The impact of global signal regression on resting state correlations: are anti-correlated networks introduced? Neuroimage 44, 893–905.
Muthén, L.K., Muthén, B.O., 1998–2010. Mplus User's Guide.
Oldfield, R.C., 1971. The assessment and analysis of handedness: the Edinburgh inventory. Neuropsychologia 9, 97–113.
Pedregosa, F., Varoquaux, G., Gramfort, A., Michel, V., Thirion, B., Grisel, O., Blondel, M., Prettenhofer, P., Weiss, R., Dubourg, V., Vanderplas, J., Passos, A., Cournapeau, D., Brucher, M., Perrot, M., Duchesnay, E., 2011. Scikit-learn: machine learning in Python. J. Mach Learn Res. 12, 2825–2830.
Peixoto, T.P., 2014. The Graph-tool Python Library. Figshare.
Power, J.D., Barnes, K.A., Snyder, A.Z., Schlaggar, B.L., Petersen, S.E., 2012. Spurious but systematic correlations in functional connectivity MRI networks arise from subject motion. Neuroimage 59, 2142–2154.
Radloff, L.S., 1977. The CES-D scale: a self-report depression scale for research in the general population. Appl. Psychol. Meas. 1, 385–401.
Raichle, M.E., MacLeod, A.M., Snyder, A.Z., Powers, W.J., Gusnard, D.A., Shulman, G.L., 2001. A default mode of brain function. Proc. Natl. Acad. Sci. U. S. A. 98, 676–682.
Ranganath, C., Ritchey, M., 2012. Two cortical systems for memory-guided behaviour. Nat. Rev. Neurosci. 13, 713–726.
Raz, N., Rodrigue, K.M., Kennedy, K.M., Land, S., 2009. Genetic and Vascular Modifiers of age-sensitive cognitive skills: effects of COMT, BDNF, ApoE, and Hypertension. Neuropsychology 23, 105–116.
Rosvall, M., Bergstrom, C.T., 2008. Maps of random walks on complex networks reveal community structure. Proc. Natl. Acad. Sci. U. S. A. 105, 1118–1123.
Rubinov, M., Sporns, O., 2011. Weight-conserving characterization of complex functional brain networks. Neuroimage 56, 2068–2079.
Sakoglu, U., Pearlson, G.D., Kiehl, K.A., Wang, Y.M., Michael, A.M., Calhoun, V.D., 2010. A method for evaluating dynamic functional network connectivity and task-modulation: application to schizophrenia. Magn. Reson. Mater. Phy 23, 351–366.
Sala-Llonch, R., Pena-Gomez, C., Arenaza-Urquijo, E.M., Vidal-Pineiro, D., Bargallo, N., Junque, C., Bartres-Faz, D., 2012. Brain connectivity during resting state and subsequent working memory task predicts behavioural performance. Cortex 48, 1187–1196.
Sambataro, F., Murty, V.P., Callicott, J.H., Tan, H.Y., Das, S., Weinberger, D.R., Mattay, V.S., 2010. Age-related alterations in default mode network: impact on working memory performance. Neurobiol. Aging 31, 839–852.
Schaefer, A., Margulies, D.S., Lohmann, G., Gorgolewski, K.J., Smallwood, J., Kiebel, S.J., Villringer, A., 2014. Dynamic network participation of functional connectivity hubs assessed by resting-state fMRI. Front Hum. Neurosci. 8.
Shakil, S., Lee, C.H., Keilholz, S.D., 2016. Evaluation of sliding window correlation performance for characterizing dynamic functional connectivity and brain states. Neuroimage 133, 111–128.
Shirer, W.R., Ryali, S., Rykhlevskaia, E., Menon, V., Greicius, M.D., 2012. Decoding subject-Driven cognitive states with whole-brain connectivity patterns. Cereb. Cortex 22, 158–165.
Shulman, G.L., Fiez, J.A., Corbetta, M., Buckner, R.L., Miezin, F.M., Raichle, M.E., Petersen, S.E., 1997. Common blood flow changes across visual tasks: II. Decreases in cerebral cortex. J. Cogn. Neurosci. 9, 648–663.
Smith, S.M., 2002. Fast robust automated brain extraction. Hum. Brain Mapp. 17, 143–155.
Smith, S.M., Fox, P.T., Miller, K.L., Glahn, D.C., Fox, P.M., Mackay, C.E., Filippini, N., Watkins, K.E., Toro, R., Laird, A.R., Beckmann, C.F., 2009. Correspondence of the brain's functional architecture during activation and rest. Proc. Natl. Acad. Sci. U. S. A. 106, 13040–13045.
Smith, S.M., Jenkinson, M., Woolrich, M.W., Beckmann, C.F., Behrens, T.E.J., Johansen-Berg, H., Bannister, P.R., De Luca, M., Drobnjak, I., Flitney, D.E., Niazy, R.K., Saunders, J., Vickers, J., Zhang, Y.Y., De Stefano, N., Brady, J.M., Matthews, P.M., 2004. Advances in functional and structural MR image analysis and implementation as FSL. Neuroimage 23, S208–S219.
Smith, S.M., Miller, K.L., Salimi-Khorshidi, G., Webster, M., Beckmann, C.F., Nichols, T.E., Ramsey, J.D., Woolrich, M.W., 2011. Network modelling methods for FMRI. Neuroimage 54, 875–891.
Stern, Y., 2002. What is cognitive reserve? Theory and research application of the reserve concept. J. Int. Neuropsych Soc. 8, 448–460.
Tibshirani, R., Walther, G., Hastie, T., 2001. Estimating the number of clusters in a data set via the gap statistic. J. Roy Stat. Soc. B 63, 411–423.
Tomasi, D., Volkow, N.D., 2012. Gender differences in brain functional connectivity density. Hum. Brain Mapp 33, 849–860.
Van Dijk, K.R.A., Sabuncu, M.R., Buckner, R.L., 2012. The influence of head motion on intrinsic functional connectivity MRI. Neuroimage 59, 431–438.
Varoquaux, G., Gramfort, A., Poline, J.-B., Thirion, B., 2010. Brain covariance selection: better individual functional connectivity models using population prior. In: Advances in Neural Information Processing Systems, pp. 2334–2342.
Wang, L., LaViolette, P., O'Keefe, K., Putcha, D., Bakkour, A., Van Dijk, K.R.A., Pihlajamaki, M., Dickerson, B.C., Sperling, R.A., 2010. Intrinsic connectivity between the hippocampus and posteromedial cortex predicts memory performance in cognitively intact older individuals. Neuroimage 51, 910–917.
Wise, R.G., Ide, K., Poulin, M.J., Tracey, I., 2004. Resting fluctuations in arterial carbon dioxide induce significant low frequency variations in BOLD signal. Neuroimage 21, 1652–1664.
Wu, J.T., Wu, H.Z., Yan, C.G., Chen, W.X., Zhang, H.Y., He, Y., Yang, H.S., 2011. Aging-related changes in the default mode network and its anti-correlated networks: a resting-state fMRI study. Neurosci. Lett. 504, 62–67.
Yin, D., Liu, W.J., Zeljic, K., Wang, Z.W., Lv, Q., Fan, M.X., Cheng, W.H., Wang, Z., 2016. Dissociable changes of frontal and parietal Cortices in Inherent functional flexibility across the human life span. J. Neurosci. 36, 10060–10074.
Yuan, P., Raz, N., 2014. Prefrontal cortex and executive functions in healthy adults: a meta-analysis of structural neuroimaging studies. Neurosci. Biobehav R. 42, 180–192.
Zalesky, A., Fornito, A., Cocchi, L., Gollo, L.L., Breakspear, M., 2014. Time-resolved resting-state brain networks. Proc. Natl. Acad. Sci. U. S. A. 111, 10341–10346.
Zhang, Y.Y., Brady, M., Smith, S., 2001. Segmentation of brain MR images through a hidden Markov random field model and the expectation-maximization algorithm. Ieee T Med. Imaging 20, 45–57.